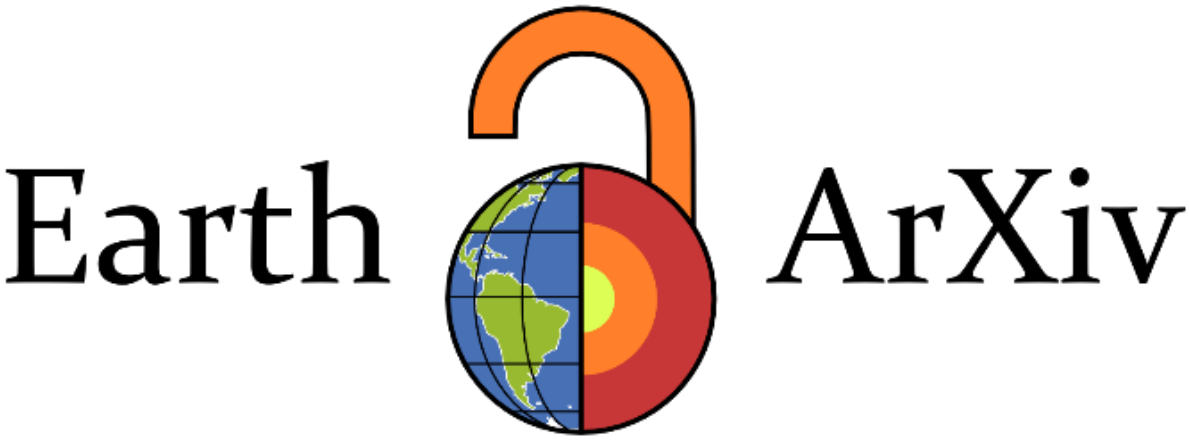

In-context learning for small-sample soil mid-infrared spectroscopy: evaluating TabPFN across an integrated soil-acidity panel

Hamza Jouichat[a,1], Lotfi Khiari[a,*,2]

[a]Department of Soil Science and Agrifood Engineering, Laval University, Quebec, QC, Canada.

* Corresponding author: lotfi.khiari@fsaa.ulaval.ca.

1 ORCID: 0000-0003-4957-2854.

2 ORCID: 0000-0003-3793-1186.

Abstract

Soil acidity diagnosis requires several interdependent laboratory measurements, limiting throughput. Mid-infrared (MIR) spectroscopy can estimate this panel from one scan, but practical use depends on robust calibration. Deep learning has surpassed conventional methods in many data-rich fields; however, adapted deep learning architectures such as convolutional neural networks (CNNs) are data-hungry and can overfit when regional datasets contain only a few hundred labelled soils. Supervised transfer learning and self-supervised learning (SSL) address this scarcity by reusing representations learned from large spectral libraries, whereas TabPFN, a newer deep-learning method designed for small tabular datasets, applies a pretrained in-context prediction rule. We tested whether TabPFN provides a stronger regional calibration strategy than these deep-learning alternatives and standard soil-spectroscopy methods. Partial least squares regression (PLSR), Cubist, 2 CNN architectures trained from scratch (SmallCNN and LargeCNN), supervised transfer, SSL and TabPFN were evaluated for ten acidity-related properties in target-specific cohorts of 418 acidic soils from eastern North America. The Open Soil Spectral Library (OSSL) supported supervised and SSL pretraining and a seven-property large-library benchmark of TabPFN and LargeCNN, with published PCA-Cubist results as an external reference. Regionally, TabPFN achieved the highest mean R^2 (0.83), followed by Cubist (0.81) and fine-tuned SSL (0.79). It led on nine properties and exceeded PLSR and both from-scratch CNNs on all ten. For the seven regional targets with corresponding or closely related measurements in OSSL, TabPFN and LargeCNN achieved mean R^2 values of 0.85 and 0.75; on OSSL, the corresponding values were 0.96 and 0.94. TabPFN's advantage over LargeCNN therefore narrowed from 0.11 regionally to 0.02 at library scale, consistent with abundant labels reducing the CNN deficit, while TabPFN remained strongest on six of seven OSSL properties. TabPFN thus offers a sample-efficient route to integrated MIR acidity assessment while retaining strong large-library performance without sample subsampling or spectral compression.

Keywords: Soil acidity; Mid-infrared spectroscopy; In-context learning; Tabular foundation model; TabPFN; Transfer learning; Self-supervised learning; Chemometrics

Highlights

- One MIR scan predicted ten acidity-related properties in 418 regional soils.
- In-context learning with TabPFN gave the highest mean R^2 (0.83) of seven methods.
- TabPFN led nine of ten properties and beat Cubist in mean R^2 (0.83 vs 0.81).
- On OSSL it led six of seven properties, with mean R^2 rising from 0.85 to 0.96.
- Its lead over LargeCNN narrowed from 0.11 regionally to 0.02 at library scale.

1. Introduction

Soil acidity is a system of properties, not a single measurement. pH in water describes active acidity, whereas buffer pH, exchangeable hydrogen and aluminium, cation-exchange capacity (CEC) and base saturation describe reserve acidity, exchange processes and the response of a soil to amendment, with organic matter and particle-size composition further governing charge and buffering. Read together, these properties give a far more complete account of acidity than pH alone, and they inform liming and soil-management decisions (Shoemaker et al., 1961). The analytical burden is equally cumulative: a conventional multi-property assessment requires several independent laboratory procedures, which constrains the throughput expected of regional testing programmes and of precision agriculture.

Mid-infrared (MIR) spectroscopy offers a way out of that burden, because a single spectrum carries information on both organic and mineral soil components (Viscarra Rossel et al., 2006), a principle established for diffuse reflectance spectroscopy across the visible to mid-infrared range (Stenberg et al., 2010). One scan could in principle return the whole acidity panel, which is what would make routine whole-profile diagnosis affordable. That requires a calibration model to learn the mapping from spectral variation to laboratory reference values, separately for every property in the panel, so how well that mapping can be learned from a regional calibration set decides whether MIR-based acidity diagnosis is practical.

Across scientific domains, mappings from complex input signals are now often best learned by deep learning, which has surpassed classical machine learning and displaced hand-designed feature extraction in fields from image analysis to molecular property prediction (LeCun et al., 2015). Convolutional neural networks (CNNs) extract local and hierarchical features directly from the input while learning the prediction function. That advantage carries a cost: the representation must itself be estimated from the training data, so conventional architectures need many examples (Mishra et al., 2022). A regional calibration set typically holds a few hundred soils, each contributing hundreds or thousands of spectral variables, so features outnumber samples by an order of magnitude or more, and under such ratios these architectures overfit

readily (Ng et al., 2020), while neural-network predictions on small pedometric datasets vary substantially across training runs (Barkov et al., 2026).

Deep learning has therefore not become the default for soil spectroscopy in the way it has elsewhere. Neural networks perform well on soil MIR where large libraries supply over ten thousand samples (Ng et al., 2019), but at regional scale the established chemometric methods remain standard practice and frequently the stronger performer (Ng et al., 2020). Partial least squares regression (PLSR) converts strongly collinear spectral variables into a few latent variables and is well matched to short, wide data (Wold et al., 2001); Cubist provides the nonlinear counterpart, combining rule-based partitions with local linear regressions (Kuhn and Quinlan, 2023). These two are the benchmark against which any new strategy for small soil datasets is tested.

Transfer learning is the established response to that constraint. A network is first trained on a large source library, and its learned filters are reused for a target dataset too small to estimate them, by fine-tuning the whole network or retraining only the final layers. Liu et al. (2018) pretrained a CNN on a large soil library and improved prediction on smaller targets; Padarian et al. (2019) localised a continental vis-NIR calibration to individual countries by fine-tuning a globally trained network, obtaining lower errors than local-only models; Mishra and Passos (2021) transferred a deep model between infrared spectrometers, recovering most of the accuracy lost to instrument differences from few fine-tuning samples. The gains are consistently largest where the target dataset is smallest. Transfer learning requires, however, that the source library carry labels for a property comparable to the target, since what transfers is a representation shaped by the source task.

Self-supervised learning removes the need for labelled source data during pretraining. The objective is built from the unlabelled spectra themselves, for example by reconstructing spectra that have been compressed or partially masked, so the feature extractor learns spectral structure without reference to any soil property. The representation is then reused by fitting a head on local labels, optionally fine-tuning part or all of the feature extractor. Wan et al. (2023) pretrained a masked autoencoder on the 19,036 NIR spectra of LUCAS 2009 and reconstructed spectra from a 188-sample regional set, raising R^2 for available nitrogen, phosphorus and potassium to 0.94, 0.93 and 0.90, between 10 and 22 per cent above the best conventional preprocessing. Sun et al. (2026) learned a 32-dimensional latent representation from 83,971 soils and predicted nine properties from the embeddings, improving on models fitted to raw MIR. The label-free objective is especially relevant for our panel, since SMP buffer pH, base saturation and exchangeable H+ are often absent from large open-access libraries, so no labelled source task exists for them.

Both pretraining routes conclude with adaptation to the regional labels, and their performance depends on the source library, pretraining objective and adaptation protocol. Foundation models provide a different approach. They are trained once, at scale, on a broad distribution of tasks and then applied to new problems. Tabular Prior-data Fitted Network (TabPFN) (Hollmann et al., 2025) trains a transformer on synthetic tabular tasks drawn from a structured prior over datasets. The resulting general-purpose regression algorithm is encoded in fixed weights and applied by in-context learning: labelled examples and query rows enter together, and one forward pass returns predictions. Barkov et al. (2026) found TabPFN to be the strongest performer across many small pedometric datasets, while identifying limits at the smallest sample sizes.

TabPFN has been applied to soil spectra by Huang et al. (2026). They drew samples from the Kellogg Soil Survey Laboratory library and predicted total carbon, pH and Olsen-extractable phosphorus, chosen to represent high, moderate and low spectral predictability. TabPFN outperformed PLSR, Cubist and a CNN in most settings, giving first evidence that in-context learning is viable for soil MIR.

This study evaluated supervised transfer learning, self-supervised learning, in-context learning with TabPFN, CNNs trained from scratch, PLSR and Cubist under a common five-fold cross-validation protocol. The regional dataset comprised ten connected acidity-related properties, seven shared with OSSL. This overlap connected the integrated regional acidity panel with a large, heterogeneous spectral library.

Accordingly, this study had three objectives: (i) to compare TabPFN with PLSR, Cubist and CNNs across ten connected acidity-related properties; (ii) to determine how in-context learning compares with SSL across all ten regional targets and with supervised transfer on the seven targets having corresponding or closely related OSSL measurements; and (iii) to contrast TabPFN and LargeCNN behaviour between the regional dataset and the much larger OSSL library, with the published PCA-Cubist workflow as an external classical benchmark.

2. Materials and methods

2.1 Study design

Each soil property was modelled under common five-fold partitions (Fig. 1). The regional analysis covered ten acidity-related properties, seven of which corresponded to or were related to OSSL properties.

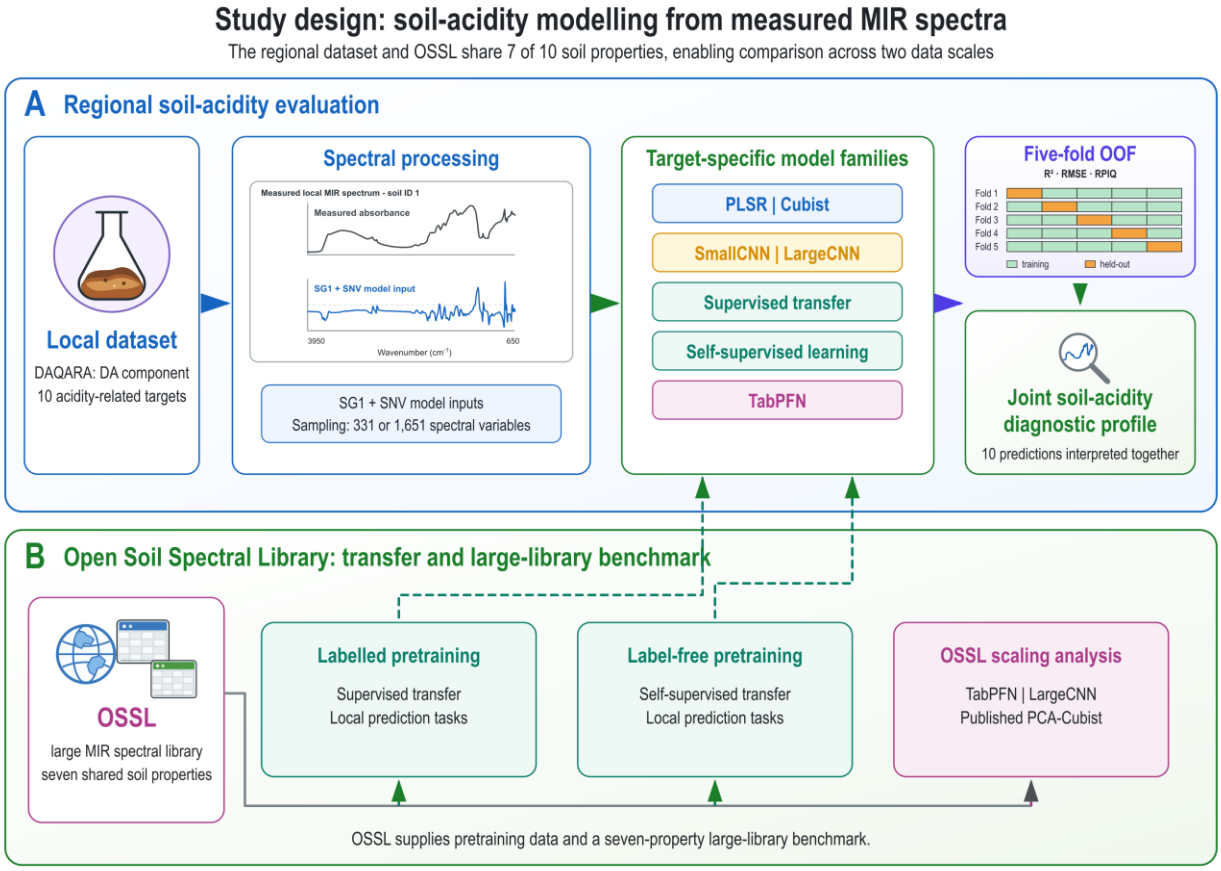

Fig. 1. Study design. (A) Ten regional acidity-related properties were modelled from Savitzky–Golay first-derivative and standard-normal-variate (SG1+SNV) MIR spectra sampled at 331 or 1,651 spectral variables. PLSR, Cubist, SmallCNN, LargeCNN, supervised transfer, self-supervised learning (SSL) and TabPFN were evaluated by five-fold cross-validation; predictions held out across the five folds formed one out-of-fold prediction vector per property. (B) The Open Soil Spectral Library (OSSL) supplied labelled and unlabelled pretraining spectra and seven properties for the large-library comparison of TabPFN, LargeCNN and the published principal-component-analysis (PCA)-Cubist benchmark. Solid arrows denote analysis and dashed arrows denote pretraining. MIR, mid-infrared; PLSR, partial least squares regression; CNN, convolutional neural network; TabPFN, tabular prior-data fitted network; R^2, coefficient of determination; RMSE, root mean squared error; RPIQ, interquartile range divided by RMSE.

2.2 Regional dataset and soil properties

The regional dataset was assembled within the soil-acidity diagnosis component of the DAQARA project. DAQARA denotes the broader decision-support research programme whose name joins Diagnostic de l'acidité (DA), Qualité des amendements (QA) and Recommandation d'application calcique (RA) - soil-acidity diagnosis, amendment-quality assessment and liming-application recommendation (Khiari, 2025).

Regional soils were collected across eastern North America. All included soils were acidic; the collection was designed for soil-acidity diagnosis rather than to span neutral and alkaline conditions. Documented provenance included 381 soils from Quebec, seven from Ontario, 15 from Prince Edward Island and 15 from Maine. MIR spectra and laboratory measurements were aligned by soil identifier, and duplicate

identifier records were consolidated before modelling. Each property-specific analytical cohort contained 418 unique soil identifiers (Table 2). Cross-validation folds were assigned at the soil level.

All ten targets contribute to acidity characterisation, although not all are direct measures of acidity. pH in water describes current acidity. SMP buffer pH reflects resistance to pH change and underpins lime-requirement frameworks (Shoemaker et al., 1961). Exchangeable H+ and Al describe components of exchangeable, or reserve, acidity, while CEC and base saturation characterise the size and occupancy of the exchange complex. Organic matter and texture affect charge, mineralogy, water relations and buffering, and so provide the context needed to interpret the direct acidity indicators. Exchangeable Al carries specific agronomic weight because aluminium toxicity is a recognised constraint on crop performance in acid soils.

Table 1. Acidity-related targets and their roles in soil-acidity diagnosis.

Target	Unit	Role in the acidity profile
pH in water	pH unit	Active acidity
SMP buffer pH	pH unit	Buffer response; lime-requirement proxy
Cation-exchange capacity	$cmol_c\ kg^{-1}$	Exchange capacity and buffering context
Base saturation	%	Occupancy of exchange sites by base cations
Exchangeable H^+	$cmol_c\ kg^{-1}$	Component of exchangeable acidity
Exchangeable Al	$cmol_c\ kg^{-1}$	Exchangeable acidity; Al stress context
Organic matter	%	Organic charge and buffering context
Clay	%	Mineral surface and buffering context
Silt	%	Particle-size context
Sand	%	Particle-size context

Note: Each property-specific analytical cohort contained 418 unique soils; SMP, Shoemaker–McLean–Pratt; cmolc kg−1, centimoles of charge per kilogram.

2.3 Regional MIR spectral acquisition

Mid-infrared absorbance spectra were acquired from dry soils ground to a particle size of 0.2 mm using a TENSOR II spectrometer (Bruker Optics) equipped with an HTS-XT high-throughput module and a mercury-cadmium-telluride detector. Spectra were exported directly from OPUS as absorbance and covered 599.79-3,997.15 cm^{-1}, with a nominal data interval of 1.43 cm^{-1} and an instrumental spectral resolution of 4 cm^{-1}. Four aliquots of each soil were loaded into separate wells and scanned independently; the four resulting spectra were averaged before modelling. Before each sample was measured, an empty well with an anodized-aluminium bottom was scanned as the reference.

2.4 OSSL spectral library and benchmark

OSSL was used as the large open soil spectral library (Safanelli et al., 2025), using the Level-1 v1.2 release. The full release contains 135,651 entries consolidated from 11 contributing soil spectral libraries. In the project copy, the MIR subset comprised 85,684 spectra from nine source libraries: KSSL (76,813), ICRAF-ISRIC (4,071), AfSIS1 (1,904), AfSIS2 (151), CAF (1,578), LUCAS-Woodwell (589), Schiedung (259), Garrett (184) and Serbia (135).

OSSL served as labelled source data for supervised transfer, an unlabelled corpus for SSL pretraining, and a large-library benchmark. Its MIR spectra were provided as pseudo-absorbance, A = log10(1/R), over 600-4,000 cm^{-1} at 2 cm^{-1} intervals. Seven properties were available for supervised transfer and benchmarking: pH in water, CEC, extractable Al, clay, sand, silt and organic carbon. Organic carbon provided a related source task for regional soil organic matter. Label-free SSL pretraining covered the complete regional panel, including SMP buffer pH, base saturation and exchangeable H^+. Target-specific benchmark sample sizes ranged from 15,710 to 82,573. OSSL and the regional dataset formed distinct evaluation settings with different soil populations, measurements and spectral acquisition.

2.5 Spectral harmonisation and preprocessing

To create comparable model inputs, the regional and OSSL wavenumber axes were sorted and spectra were linearly interpolated over the common range of 650–3,950 cm^{-1}. Sampling at 10 and 2 cm^{-1} yielded 331 and 1,651 points, respectively. These inputs are hereafter termed coarse sampling (331 points) and fine sampling (1,651 points). The terms describe numerical model inputs, not instrumental optical resolution.

Each interpolated spectrum was transformed using an 11-point, second-order Savitzky-Golay first derivative (Savitzky and Golay, 1964), followed by spectrum-wise standard normal variate normalisation (Barnes et al., 1989). This SG1+SNV transformation centres each spectrum on its mean and scales it by its standard deviation. Hereafter, SG1+SNV-transformed spectra are termed processed spectra.

2.6 Prediction models

2.6.1 PLSR and Cubist

PLSR and Cubist were fitted independently for each regional soil property. Hyperparameters were selected by inner cross-validation within each outer training fold: 2-50 latent components for PLSR, and 1, 5, 10 or 20 committees combined with 0, 5 or 9 neighbours for Cubist. Both methods were evaluated on processed spectra with coarse and fine sampling.

At OSSL scale, the classical benchmark was the published Cubist workflow of Safanelli et al. (2025). Cubist's computational cost increases with sample count, predictor count and the number of committees, as also observed in pilot end-to-end runs using OSSL spectra at fine sampling. Safanelli et al. controlled this cost by applying SNV, reducing the spectra to 120 principal components that retained approximately 99% of the variance, and selecting the committee count on subsets of about 2,000 samples before fitting the selected model to the full training data. The OSSL scaling analysis compared this published workflow with TabPFN and LargeCNN evaluated on processed spectra with fine sampling.

2.6.2 CNN training from scratch

Both from-scratch CNNs were fitted separately for each regional property using processed spectra with coarse and fine sampling. The two sampling densities evaluated the effect of spectral input density, while the two architectures evaluated whether a compact convolutional model benefited the small regional calibration set (Fig. 2). LargeCNN comprised four convolutional blocks with 32, 64, 128 and 256 feature maps; each block used kernel size 20, same padding, rectified-linear activation and max-pooling, with pooling factors 2, 5, 5 and 2. The resulting representation passed through dropout, a 100-unit dense layer, a second dropout layer and a scalar output.

SmallCNN was designed as a more strongly regularised alternative, with three convolutional blocks of 16, 32 and 64 feature maps, decreasing kernel sizes of 15, 11 and 7, batch normalisation, and 2:1 max-pooling after the first two blocks. Global average pooling (GAP) then reduced each learned feature map to a single value before a 32-unit dense layer and scalar output. Replacing the large flattened representation with GAP substantially reduces the size of the regression head. The design hypothesis was that this compact architecture would suit a few hundred local samples better; the comparison is therefore a deliberate architectural test.

A separate network was trained per target with the Adam optimiser and mean-squared-error loss, using a learning rate of 10^{-3}, batch size 16, at most 200 epochs, and early stopping on a validation subset drawn only from the current training fold. Input and target scaling parameters were estimated from training data alone.

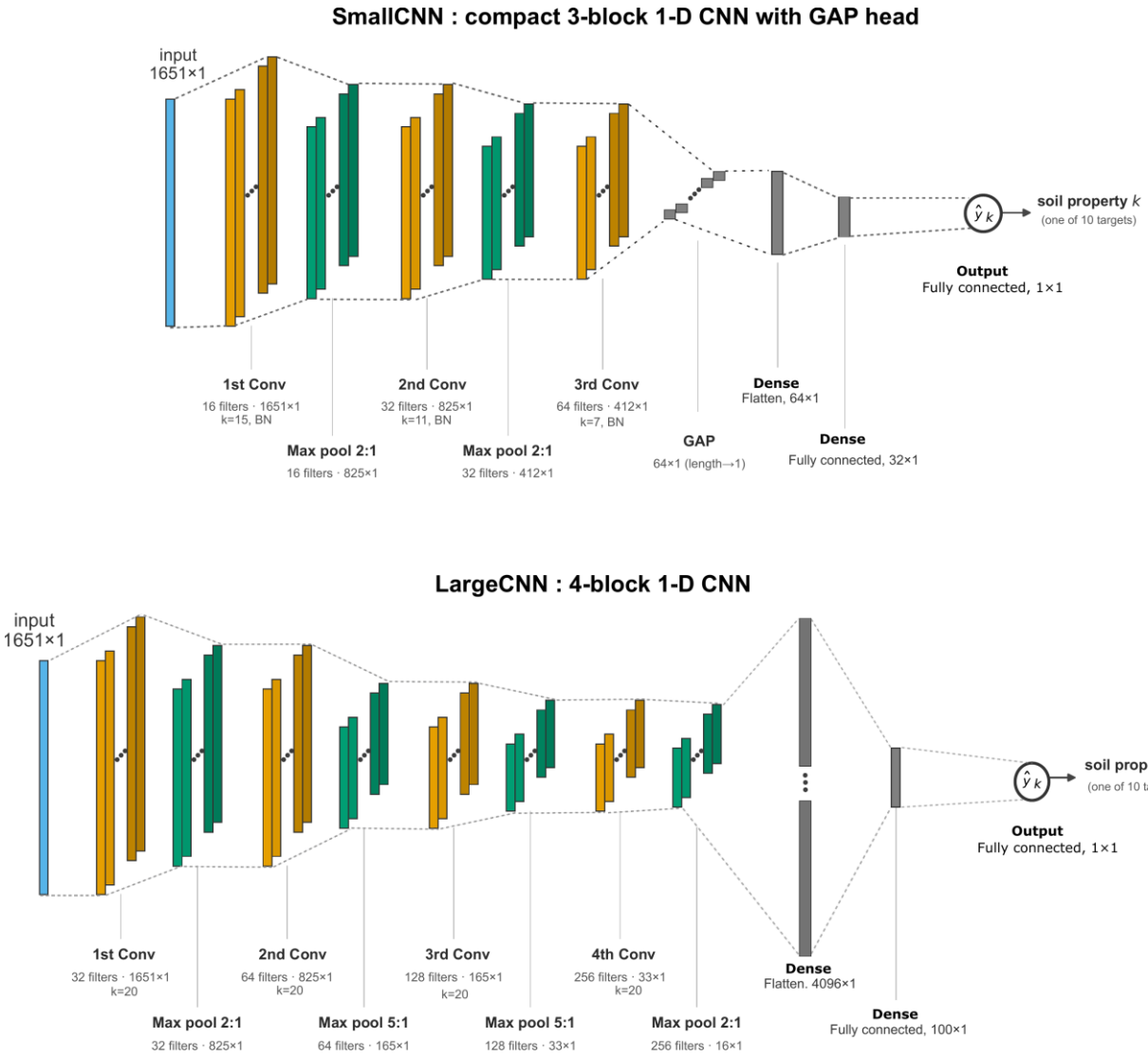

Fig. 2. SmallCNN and LargeCNN architectures trained from scratch for each regional target. The schematic shows SG1+SNV-processed spectra with fine sampling (1,651 points); both networks were also evaluated with coarse sampling (331 points). Bars represent feature maps, dotted outlines show dimensional changes, and $\hat{y}_k$ is the prediction for target k. SmallCNN uses GAP, whereas LargeCNN uses a flattened dense head. CNN, one-dimensional convolutional neural network; SG1+SNV, Savitzky-Golay first derivative plus standard normal variate; Conv, convolutional block; BN, batch normalisation; GAP, global average pooling; FC, fully connected; k, kernel size.

2.6.3 Supervised transfer learning

For seven corresponding or related target pairs, a single-target LargeCNN was first trained on OSSL processed spectra with fine sampling (Fig. 3). In the frozen variant, non-head parameters were held fixed while the loaded prediction head was updated on local data; in the fine-tuned variant all parameters were updated. Local adaptation used a learning rate of 10^{-4}, batch size 16, at most 100 epochs, and early stopping.

The source-trained network supplied whole-model initialisation, including the prediction head. The inherited head therefore retained information about the source target and its scale, which is relevant when source and regional target definitions differ, as for OSSL organic carbon and regional organic matter.

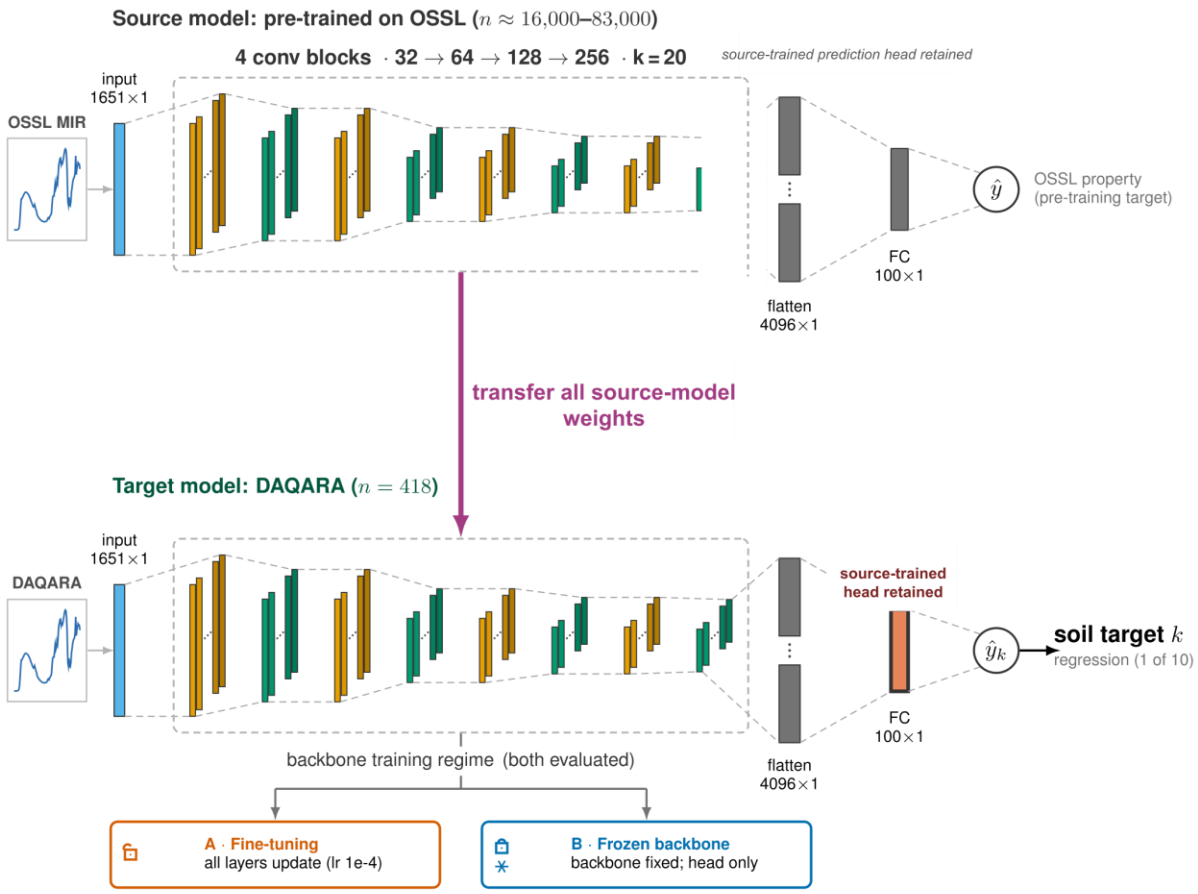

Fig. 3. Supervised whole-model transfer with LargeCNN. Separate source models were trained on OSSL SG1+SNV MIR spectra for seven corresponding or related properties (n ≈ 16,000–83,000). Each source model, including its prediction head, initialised the regional model; fine-tuning updated all layers (learning rate, 10−4), whereas frozen adaptation updated only the head. Each regional cohort comprised 418 soils (n = 418). OSSL, Open Soil Spectral Library; MIR, mid-infrared; SG1+SNV, Savitzky–Golay first derivative plus standard normal variate; CNN, convolutional neural network; Conv, convolutional block; FC, fully connected; k, kernel size; ŷk, prediction for property k.

2.6.4 Self-supervised pretraining

SSL used OSSL spectra without property labels (Fig. 4). The LargeCNN feature extractor acted as encoder, a linear bottleneck reduced the representation to 32 values, and a decoder reconstructed each processed spectrum at fine sampling, with reconstruction mean squared error as the pretraining signal. The bottleneck and decoder were discarded before regression on local data. The prediction head stored with the encoder had not participated in reconstruction training and so remained at its random initialisation before local

adaptation. Frozen SSL updated the local head while holding the feature extractor fixed; fine-tuned SSL updated the full prediction model.

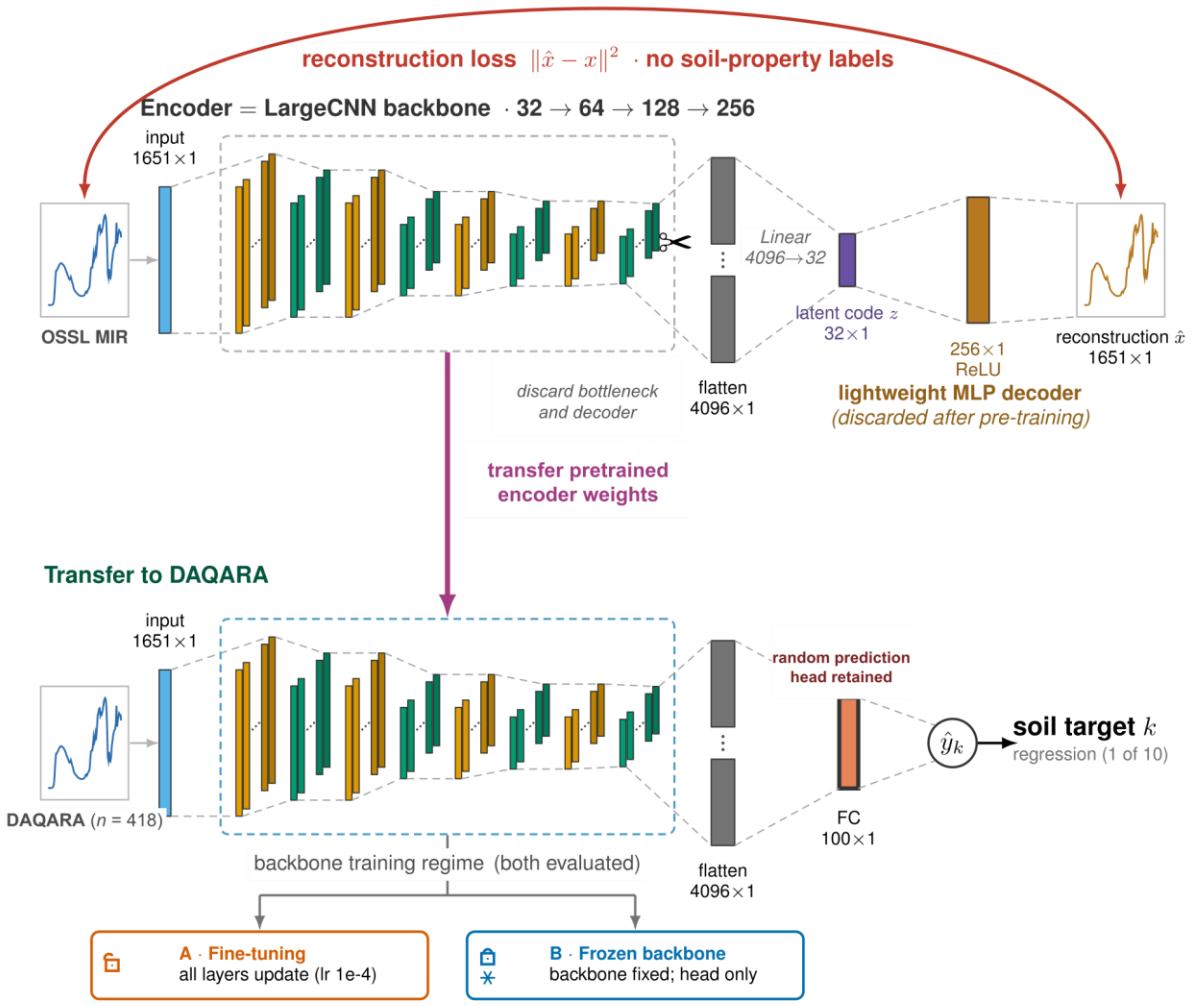

Fig. 4. Label-free self-supervised learning (SSL) and transfer with LargeCNN. OSSL SG1+SNV MIR spectra were encoded to a 32-value latent representation and reconstructed without property labels. The bottleneck and decoder were discarded before regional prediction (n = 418); fine-tuning updated all layers (learning rate, 10−4), whereas frozen adaptation updated only the prediction head. OSSL, Open Soil Spectral Library; MIR, mid-infrared; SG1+SNV, Savitzky–Golay first derivative plus standard normal variate; CNN, convolutional neural network; MLP, multilayer perceptron; ReLU, rectified linear unit; FC, fully connected; x, input spectrum; x̂, reconstruction; z, latent representation; ŷk, prediction for property k.

2.6.5 TabPFN and in-context learning

A foundation model is pretrained once on a broad collection of tasks and reused across datasets. For the tabular foundation model TabPFN (Hollmann et al., 2025; Prior Labs, 2026), pretraining uses synthetic tables generated from a designed statistical prior representing many possible relationships between predictors and targets. By learning to solve many such tasks, the transformer encodes a general prediction

rule in its fixed weights. Attention gives greater weight to relevant parts of the input; in TabPFN it operates across samples and features, relating each query to the labelled examples and spectral variables supplied with it (Hollmann et al., 2025).

In-context learning applies the pretrained rule to a new prediction problem. The model receives a context set containing predictors and known target values together with query rows whose targets are withheld. The context serves as the calibration set and is read as model input while the pretrained weights remain fixed. Supervised transfer and SSL use the regional data to update CNN weights.

In-context learning requires the labelled context to fit within the model's supported combination of rows and features. TabPFN-3 expands this capacity to documented limits of 1,000,000 × 200, 100,000 × 2,000 or 1,000 × 20,000 rows × features (Grinsztajn et al., 2026). The regional dataset and the largest OSSL task (82,573 soils) fall within these limits under fine sampling (1,651 features).

TabPFN was implemented in Python 3.11.15 using tabpfn v8.0.7 and the default TabPFN-3 regression checkpoint.

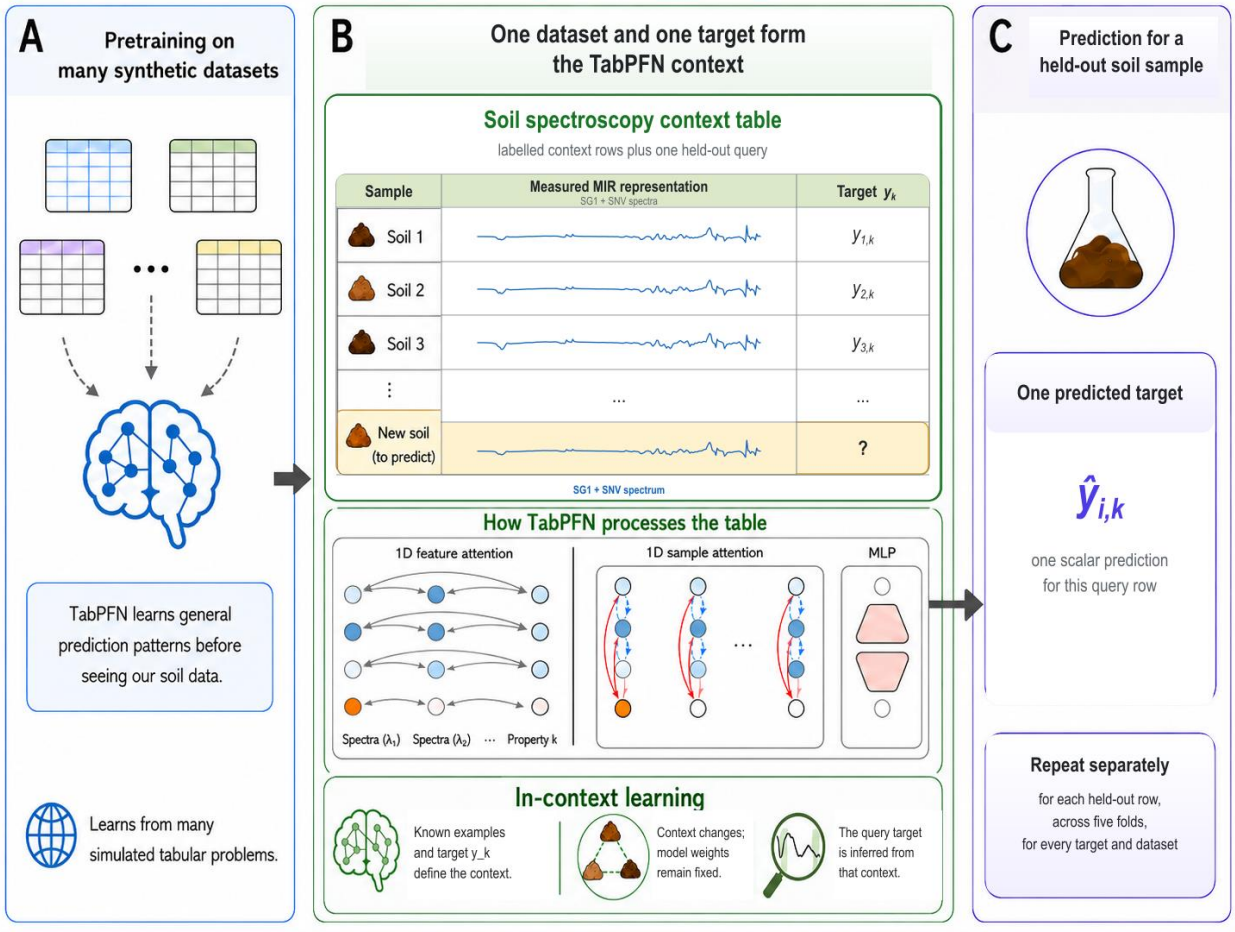

Fig. 5. TabPFN in-context prediction. (A) TabPFN is pretrained on synthetic tabular tasks. (B) For property k, SG1+SNV MIR spectra and observed values $y_{i,k}$ from four folds form the labelled context; spectra from the held-out fold are queries. Feature and

sample attention followed by a multilayer perceptron returns predictions $\hat{y}_{i,k}$. (C) Fixed model weights are used across five folds, all properties and both datasets. TabPFN, tabular prior-data fitted network; MIR, mid-infrared; SG1+SNV, Savitzky-Golay first derivative plus standard normal variate; MLP, multilayer perceptron; OSSL, Open Soil Spectral Library.

2.7 Cross-validation and performance evaluation

Regional and within-study OSSL performance was estimated by shuffled five-fold cross-validation (random seed 42), with folds defined at the soil level. In each iteration, four folds formed the training partition and the fifth formed the assessment partition. Model fitting and, where applicable, learned scaling, hyperparameter selection and early-stopping validation were confined to the training partition. The five assessment-fold predictions were then pooled, giving every eligible soil one out-of-fold prediction.

Regional models were compared on common target-specific cohorts and folds. The primary comparison examined processed spectra at fine sampling; the sampling analysis retained the same folds and model settings while changing the input from 331 to 1,651 spectral variables. Within OSSL, TabPFN and LargeCNN were evaluated on the same property-specific samples and inputs. Published PCA-Cubist results were retained as an external benchmark because their preprocessing and validation protocol differed.

For each property, metrics were calculated from the pooled out-of-fold observations and predictions. Let y_i and $\hat{y}_i$ denote the observed and predicted values for eligible soil i, $\bar{y}$ the mean of all pooled observations for that property, n the target-specific sample size, and $Q_{0.75}(y)$ and $Q_{0.25}(y)$ the third and first quartiles of the pooled observed values for that property. Eqs. (1)–(3) define the three performance metrics.

$$R^2 = 1 - \frac{\sum_{i=1}^{n}(y_i - \hat{y}_i)^2}{\sum_{i=1}^{n}(y_i - \bar{y})^2} \quad (1)$$

$$\mathrm{RMSE} = \sqrt{\frac{1}{n}\sum_{i=1}^{n}(y_i - \hat{y}_i)^2} \quad (2)$$

$$\mathrm{RPIQ} = \frac{Q_{0.75}(y) - Q_{0.25}(y)}{\mathrm{RMSE}} \quad (3)$$

The coefficient of determination (R^2) was the primary metric. RMSE expresses prediction error in the target unit, whereas RPIQ scales RMSE by the observed interquartile range. Higher R^2 and RPIQ and lower RMSE indicate better performance. For each pooled metric, 95% confidence intervals were obtained from 2,000 nonparametric bootstrap resamples of soil identifiers, using the 2.5th and 97.5th percentiles. The same resampled identifiers were applied to matched models within each property, preserving paired comparisons. Cross-property summaries are unweighted means of the property-level

pooled R^2 or RPIQ values; their intervals were calculated by averaging the corresponding bootstrap replicates. RMSE was not averaged across properties because target units differ.

3. Results

3.1 Regional prediction performance

TabPFN had the highest cross-property pooled R^2 (0.83; 95% bootstrap CI, 0.81–0.85) and RPIQ (2.30; 2.18–2.49) at fine sampling (Table 2). Cubist was the closest comparator (R^2, 0.81; 0.79–0.83), followed by fine-tuned SSL (0.79; 0.77–0.81). The intervals show that several individual-property rankings were close, but TabPFN's advantage was repeated across the panel.

TabPFN led nine of ten properties, spanning pH, buffered and exchangeable acidity, the exchange complex and all three texture fractions. It was strongest for CEC (R^2 = 0.98) and also predicted organic matter well (0.96), although fine-tuned SSL and Cubist were slightly better for that property. The compact SmallCNN did not provide the expected small-sample advantage and remained below LargeCNN for every property.

RMSE expressed these differences in the units of each soil property. For the four direct acidity indicators, TabPFN errors were 0.30 pH unit for pH in water, 0.23 pH unit for SMP buffer pH, 0.12 cmolc kg^{-1} for exchangeable H+ and 0.22 cmolc kg−1 for exchangeable Al. Relative to LargeCNN, TabPFN reduced RMSE for every property; the largest relative reductions occurred for CEC (3.51 versus 5.66 cmolc kg−1; 38%) and pH in water (0.30 versus 0.43 pH unit; 30%).

Table 2 reports the fine-tuned supervised-transfer and SSL models, which had the strongest average performance within their respective transfer strategies. With the feature extractor frozen and only the prediction head updated, mean pooled R^2 was 0.75 for supervised transfer across seven eligible properties and 0.77 for SSL across all ten properties. Full-network fine-tuning increased these values to 0.80 and 0.79, respectively. Among the seven properties eligible for both approaches, SSL produced the higher R^2 for six; CEC was the exception.

Table 2. Regional predictive performance of seven modelling approaches across ten acidity-related soil properties.

Target (RMSE unit; n)	Metric	PLSR	Cubist	Small CNN	Large CNN	Sup. TL (ft)	SSL (ft)	TabPFN
pH in water (pH) (n = 418)	R^2	0.68	0.77	0.35	0.56	0.64	0.69	**0.79**
	RMSE	0.37	0.31	0.52	0.43	0.39	0.36	**0.30**
	RPIQ	2.50	2.94	1.75	2.14	2.35	2.52	**3.08**
SMP buffer pH (pH) (n = 418)	R^2	0.67	0.72	0.46	0.64	—	0.71	**0.74**
	RMSE	0.26	0.24	0.33	0.27	—	0.25	**0.23**

Target (RMSE unit; n)	Metric	PLSR	Cubist	Small CNN	Large CNN	Sup. TL (ft)	SSL (ft)	TabPFN
	RPIQ	1.81	1.99	1.43	1.75	—	1.94	**2.05**
Exch. H+ (cmolc kg−1) (n = 418)	R^2	0.63	0.73	0.46	0.68	—	0.72	**0.78**
	RMSE	0.15	0.13	0.19	0.15	—	0.13	**0.12**
	RPIQ	0.81	0.94	0.67	0.86	—	0.93	**1.03**
Exch. Al (cmolc kg−1) (n = 418)	R^2	0.62	0.79	0.39	0.70	0.79	0.80	**0.84**
	RMSE	0.34	0.25	0.44	0.31	0.25	0.25	**0.22**
	RPIQ	0.29	0.39	0.23	0.33	0.40	0.40	**0.45**
Base saturation (% pts) (n = 418)	R^2	0.75	0.83	0.30	0.78	—	0.81	**0.86**
	RMSE	12.34	10.26	20.60	11.45	—	10.82	**9.31**
	RPIQ	2.32	2.79	1.39	2.50	—	2.65	**3.07**
CEC (cmolc kg−1) (n = 418)	R^2	0.97	0.97	0.84	0.95	0.97	0.96	**0.98**
	RMSE	4.58	4.20	9.84	5.66	4.25	4.79	**3.51**
	RPIQ	2.79	3.04	1.30	2.25	3.01	2.67	**3.64**
Organic matter (% pts) (n = 418)	R^2	0.96	0.97	0.57	0.96	0.96	**0.98**	0.96
	RMSE	1.90	1.48	5.96	1.82	1.72	**1.40**	1.80
	RPIQ	1.56	2.00	0.50	1.62	1.72	**2.11**	1.65
Clay (% pts) (n = 418)	R^2	0.80	0.83	0.71	0.76	0.80	0.83	**0.86**
	RMSE	5.20	4.72	6.16	5.64	5.12	4.78	**4.38**
	RPIQ	1.79	1.97	1.51	1.65	1.82	1.95	**2.12**
Silt (% pts) (n = 418)	R^2	0.65	0.70	0.54	0.58	0.65	0.67	**0.72**
	RMSE	8.91	8.19	10.15	9.67	8.79	8.61	**7.89**
	RPIQ	2.34	2.55	2.05	2.16	2.37	2.42	**2.64**
Sand (% pts) (n = 418)	R^2	0.74	0.79	0.68	0.72	0.76	0.77	**0.81**
	RMSE	10.65	9.56	11.82	11.18	10.18	10.11	**9.06**
	RPIQ	2.79	3.11	2.51	2.66	2.92	2.94	**3.28**
Unweighted mean (ten targets)	R^2	0.75	0.81	0.53	0.73	0.80†	0.79	**0.83**
	RPIQ	1.90	2.17	1.33	1.79	2.08†	2.05	**2.30**

Note: Values are pooled five-fold out-of-fold estimates; n is the property-specific number of unique soils; all models received SG1+SNV MIR spectra at fine sampling (1,651 spectral variables); PLSR, partial least squares regression; SSL (ft), fine-tuned self-supervised learning; Sup. TL (ft), fine-tuned supervised transfer learning, available only for the seven corresponding or related OSSL targets; OSSL, Open Soil Spectral

Target (RMSE unit; n)	Metric	PLSR	Cubist	Small CNN	Large CNN	Sup. TL (ft)	SSL (ft)	TabPFN

Library; CEC, cation-exchange capacity; SG1+SNV, Savitzky–Golay first derivative plus standard normal variate; R^2 and RPIQ are dimensionless and increase with performance; RMSE retains the target unit and decreases with performance; em dash (—) denotes a property with no corresponding OSSL source label; cross-property summaries are unweighted means across the ten targets; RMSE is not averaged across properties because target units differ; bold indicates the best unrounded estimate in each row. † Supervised-transfer summaries cover the seven eligible properties only and are not directly comparable with the ten-property means.

3.2 Effect of spectral sampling

The sampling analysis changed only the processed spectral input from 331 to 1,651 variables while retaining target cohorts, folds and model settings (Table 3). Table 2 gives the corresponding fine-sampling estimates.

The effects of finer spectral sampling were model dependent. TabPFN improved R^2 for nine of ten properties (mean $\Delta R^2 = +0.018$), with the clearest gains for pH in water and the texture fractions; RMSE also decreased for those same nine properties. CEC was the only exception: R^2 changed by −0.003 and RMSE increased by 0.24 cmolc kg−1. Cubist improved both R^2 and RMSE for eight properties (mean $\Delta R^2 = +0.009$). PLSR and LargeCNN showed negligible mean R^2 changes (+0.005 for each), with gains and losses varying among properties. SmallCNN deteriorated for seven properties (mean $\Delta R^2 = -0.074$), with pronounced losses for base saturation, exchangeable acidity and organic matter.

Table 3. Change in regional predictive performance when spectral sampling increased from 331 to 1,651 variables.

Target (RMSE unit)	Change	PLSR	Cubist	Small CNN	Large CNN	TabPFN
pH in water (pH) (n = 418)	ΔR^2	+0.060	+0.010	+0.034	−0.001	+0.036
	ΔRMSE	−0.033	−0.007	−0.014	0.000	−0.025
	ΔRPIQ	+0.207	+0.064	+0.044	−0.001	+0.234
SMP buffer pH (pH) (n = 418)	ΔR^2	+0.011	−0.008	−0.013	+0.017	+0.012
	ΔRMSE	−0.004	+0.004	+0.004	−0.006	−0.005
	ΔRPIQ	+0.030	−0.031	−0.017	+0.039	+0.046
Exch. H+ (cmolc kg−1) (n = 418)	ΔR^2	0.000	+0.009	−0.094	+0.018	+0.052
	ΔRMSE	0.000	−0.002	+0.017	−0.004	−0.013
	ΔRPIQ	0.000	+0.015	−0.067	+0.023	+0.103
Exch. Al (cmolc kg−1) (n = 418)	ΔR^2	−0.024	+0.014	−0.196	−0.023	+0.002
	ΔRMSE	+0.011	−0.008	+0.076	+0.012	−0.002
	ΔRPIQ	−0.010	+0.013	−0.049	−0.013	+0.003

Target (RMSE unit)	Change	PLSR	Cubist	Small CNN	Large CNN	TabPFN
Base saturation (% pts) (n = 418)	ΔR²	−0.015	−0.006	−0.182	+0.075	+0.010
	ΔRMSE	+0.373	+0.180	+2.863	−1.823	−0.319
	ΔRPIQ	−0.072	−0.050	−0.224	+0.343	+0.102
CEC (cmolc kg−1) (n = 418)	ΔR²	+0.004	+0.003	−0.032	+0.014	−0.003
	ΔRMSE	−0.252	−0.186	+1.063	−0.728	+0.237
	ΔRPIQ	+0.146	+0.129	−0.157	+0.257	−0.264
Organic matter (% pts) (n = 418)	ΔR²	+0.004	+0.037	−0.296	−0.004	+0.005
	ΔRMSE	−0.079	−0.814	+2.628	+0.100	−0.113
	ΔRPIQ	+0.063	+0.707	−0.392	−0.095	+0.098
Clay (% pts) (n = 418)	ΔR²	+0.038	+0.013	−0.016	−0.033	+0.015
	ΔRMSE	−0.463	−0.182	+0.177	+0.404	−0.219
	ΔRPIQ	+0.146	+0.073	−0.045	−0.128	+0.101
Silt (% pts) (n = 418)	ΔR²	−0.011	+0.012	+0.018	−0.019	+0.024
	ΔRMSE	+0.145	−0.160	−0.196	+0.220	−0.335
	ΔRPIQ	−0.039	+0.049	+0.039	−0.050	+0.108
Sand (% pts) (n = 418)	ΔR²	−0.012	+0.004	+0.040	+0.002	+0.023
	ΔRMSE	+0.241	−0.099	−0.725	−0.042	−0.532
	ΔRPIQ	−0.064	+0.032	+0.145	+0.010	+0.182
Unweighted mean (ten targets)	ΔR²	+0.005	+0.009	−0.074	+0.005	+0.018
	ΔRPIQ	+0.041	+0.100	−0.072	+0.038	+0.071

Note: Δ = fine sampling − coarse sampling, from pooled five-fold out-of-fold estimates; target cohorts, folds and model settings were held constant; PLSR, partial least squares regression; CEC, cation-exchange capacity; positive ΔR² and ΔRPIQ and negative ΔRMSE indicate improvement; RMSE retains the target unit; summary rows give the unweighted mean Δ across the ten properties.

3.3 OSSL benchmark performance

At OSSL scale, TabPFN increased the seven-property mean pooled R^2 to 0.96 and led LargeCNN on six properties (Table 4). LargeCNN reached 0.94 on average and was slightly better only for organic carbon. Its large-library performance was substantially stronger than its regional result, consistent with CNN representation learning benefiting from abundant labelled spectra. Both within-study means exceeded the published PCA-Cubist R^2 mean, although that benchmark followed a different preprocessing and validation protocol.

Performance differences between the regional and OSSL evaluations depended on model family. LargeCNN's mean pooled R^2 was 0.75 in the regional dataset and 0.94 in OSSL, whereas TabPFN reached 0.85 and 0.96, respectively. TabPFN's advantage over LargeCNN therefore narrowed from 0.11 R^2 units regionally to 0.02 at OSSL scale. The regional calibration was not uniformly weaker: for CEC, TabPFN achieved $R^2 = 0.98$, RMSE = 3.51 cmolc kg−1 and RPIQ = 3.64, compared with 0.95, 5.10 cmolc kg−1 and 3.31 on OSSL. For pH in water, RMSE differed by only 0.04 pH unit (0.30 versus 0.26), despite larger differences in R^2 and RPIQ.

Within OSSL, TabPFN reduced RMSE relative to LargeCNN for six of seven properties: by 8% for CEC and by 14–20% for pH, extractable Al and the three texture fractions. Organic carbon was the exception, for which LargeCNN achieved a lower RMSE than TabPFN (1.15 versus 1.38 percentage points).

Table 4. Predictive performance on the OSSL library for seven soil properties.

OSSL target (RMSE unit; n)	Metric	LargeCNN Fine sampling	TabPFN Fine sampling	Published PCA-Cubist
Extractable Al (cmolc kg−1) (n = 15,710)	R^2	0.91	**0.94**	0.90
	RMSE	1.02	**0.87**	0.23†
	RPIQ	2.52	**2.96**	4.74†
CEC (cmolc kg−1) (n = 57,651)	R^2	0.94	**0.95**	0.96
	RMSE	5.53	**5.10**	0.17†
	RPIQ	3.05	**3.31**	6.12†
Clay (% pts) (n = 57,268)	R^2	0.940	**0.961**	0.90
	RMSE	4.30	**3.47**	5.64
	RPIQ	5.51	**6.82**	4.20
Organic carbon (% pts) (n = 82,573)	R^2	**0.993**	0.989	0.99
	RMSE	**1.15**	1.38	0.12†
	RPIQ	**2.74**	2.28	9.98†
pH in water (pH) (n = 59,997)	R^2	0.943	**0.961**	0.91
	RMSE	0.32	**0.26**	0.40
	RPIQ	7.03	**8.54**	5.63
Sand (% pts) (n = 57,162)	R^2	0.949	**0.968**	0.92
	RMSE	6.50	**5.20**	8.33
	RPIQ	7.49	**9.36**	5.84

OSSL target (RMSE unit; n)	Metric	LargeCNN Fine sampling	TabPFN Fine sampling	Published PCA-Cubist
Silt (% pts) (n = 57,215)	R^2	0.92	**0.95**	0.88
	RMSE	5.70	**4.64**	7.31
	RPIQ	5.65	**6.93**	4.40
Unweighted mean (seven targets)	R^2	0.94	**0.96**	0.92

Note: Within-study values are pooled five-fold out-of-fold estimates; LargeCNN and TabPFN were evaluated on identical SG1+SNV MIR inputs at fine sampling; OSSL, Open Soil Spectral Library; PCA, principal component analysis; CEC, cation-exchange capacity; SG1+SNV, Savitzky–Golay first derivative plus standard normal variate; published PCA-Cubist values are from Safanelli et al. (2025), who applied standard normal variate transformation and 120 principal components, tuned committees by inner five-fold cross-validation, and reported metrics from ten-fold cross-validation with refitting, so they are not directly comparable with the within-study columns; R^2 and RPIQ increase with performance; RMSE decreases; bold compares the two within-study models. † RMSE and RPIQ for extractable Al, CEC and organic carbon were calculated after log1p transformation; other errors retain the displayed target units.

4. Discussion

4.1 In-context learning under regional data constraints

The regional results point to sample efficiency as the main strength of TabPFN in this setting. Both from-scratch CNNs had to learn a spectral representation and a property-specific regression function from each regional training fold, and the poorer performance of SmallCNN indicates that reducing model capacity alone did not overcome this constraint. This agrees with soil-spectroscopy learning curves showing that CNNs become increasingly effective as calibration datasets grow to several thousand spectra (Ng et al., 2020).

TabPFN also relies on a high-capacity transformer architecture (Vaswani et al., 2017), whose success across deep-learning domains has largely depended on extensive pretraining (Dosovitskiy et al., 2021). Its transformer was pretrained on millions of synthetic tabular datasets to learn a general prediction procedure (Hollmann et al., 2025), shifting this data-intensive learning stage away from the regional calibration. During evaluation here, the labelled regional spectra specified each soil-property relationship as context while the pretrained weights remained fixed. This provides a plausible explanation for TabPFN's strong performance with only a few hundred local observations and high-dimensional MIR inputs.

TabPFN's gains varied by target, with Cubist close overall and organic matter favouring other models. Still, the regional results support prior-data pretraining for limited local calibration, consistent with Barkov et al. (2026).

4.2 Supervised transfer and self-supervised pretraining

Among the OSSL-based strategies, SSL transferred more consistently than supervised pretraining, exceeding it on six of the seven matched targets. This favours label-free pretraining for a heterogeneous acidity panel, where source–target correspondence varies among properties and several regional targets have no equivalent OSSL label. Similar transferability of self-supervised spectral representations has been reported by Wan et al. (2023) and Sun et al. (2026). The CEC exception nevertheless shows that supervised transfer remains competitive when source and target measurements align closely.

TabPFN provided a stronger regional alternative. Unlike SSL and supervised transfer, which require an external soil spectral library and a dedicated pretraining or fine-tuning stage, TabPFN needs no additional training or gradient-based optimisation at application time. It outperformed SSL overall without requiring a user-supplied source library or target-specific optimisation. This simplifies regional calibration, as labelled soils can be used directly as context for a fixed pretrained model. Thus, while SSL reduces dependence on source labels, TabPFN removes the need for locally managed pretraining procedures, combining stronger performance with a simpler workflow.

4.3 Effects of spectral sampling

The value of finer spectral sampling was model dependent. TabPFN benefited most consistently from the 1,651-variable input, Cubist showed smaller gains, and PLSR and LargeCNN changed little overall. SmallCNN showed the opposite pattern, performing better with the coarser representation. Similar model dependence has been reported in soil spectroscopy: spectral downsampling reduced CNN accuracy in the large LUCAS dataset (Zhong et al., 2021), whereas coarser representations retained comparable performance with Cubist for several soil properties (Behrens et al., 2022). Thus, additional spectral detail is useful only when the modelling approach can exploit it effectively.

4.4 Comparison with published MIR calibrations

TabPFN's regional accuracy compares favourably with established MIR calibrations. Hume et al. (2024) reported R^2 values of 0.74 for pH in water, 0.71 for exchangeable Al and 0.76 for CEC in an acidic-soil calibration, compared with 0.79, 0.84 and 0.98 here. The CEC result is particularly strong, while the R^2 of 0.86 for base saturation contrasts with the poor prediction reported by Baumann et al. (2021; $R^2 = 0.24$). TabPFN also reached 0.86, 0.72 and 0.81 for clay, silt and sand, respectively, compared with 0.81, 0.41 and 0.45 in Baumann et al. (2021). Higher values have been reported for individual targets in smaller local datasets, including $R^2 = 0.91$ for pH and 0.90 for silt and sand after interval selection by Mokere et al. (2026). Taken together, these results place TabPFN among the leading regional MIR approaches,

combining strong performance across the acidity panel with a simple in-context workflow that requires no task-specific tuning.

The large-library benchmark supports the same conclusion at a different scale. On OSSL, TabPFN achieved a mean R^2 of 0.96 and led LargeCNN on six of seven properties. It also exceeded the published PCA-Cubist R^2 for extractable Al, clay, pH, sand and silt, while essentially matching organic carbon and trailing slightly for CEC (Safanelli et al., 2025). Although the published Cubist results used a different validation and preprocessing workflow, the comparison places TabPFN among the strongest reported MIR models at library scale as well as regionally.

4.5 Scaling to large spectral libraries and soil foundation models

The OSSL experiment extends in-context learning from regional calibration to library-scale soil spectroscopy. TabPFN-3 handled up to 82,573 soils and 1,651 spectral variables with fixed pretrained weights, using the labelled spectra directly as context rather than fitting a new model for each task. This was previously difficult for TabPFN: earlier applications to high-dimensional spectral inputs, including vis-NIR, NIR and MIR, applied principal component analysis to manage the unfavourable feature-to-sample ratio (Barkov et al., 2026). These results show the potential of foundation models to provide accurate, scalable, and low-overhead calibration strategies and point to domain-specific foundation models as a promising direction for future soil-spectroscopy research. Recent work illustrates what soil-specific pretraining could add to this direction. Leng et al. (2026) developed SoilFormer on large multimodal soil–environment data and showed that the pretrained model could reconstruct partially observed soil properties with uncertainty estimates while recovering established relationships among properties such as pH, texture and soil organic carbon. Building on the performance demonstrated here, future work could therefore investigate whether soil-specific pretraining can further improve generalisation while incorporating soil-system structure and predictive uncertainty.

4.6 Limitations and future validation

The regional evaluation was confined to an acidity-focused population from eastern North America, so its performance should not be assumed to extend to neutral or alkaline soils. Random soil-level cross-validation estimates performance within the sampled population, whereas site, field or profile-grouped validation is needed to establish geographic transfer. The present study also evaluated point predictions only. Future validation should therefore test predictive uncertainty, agreement at agronomic thresholds, and whether the resulting errors preserve lime-management decisions under prospective use.

5. Conclusion

A complete soil-acidity diagnosis requires analyzing multiple soil properties. This study shows that a single MIR spectrum, combined with in-context learning, can support prediction of ten complementary acidity-related properties in a regional soil population. TabPFN provided the most consistent regional performance, leading nine properties and achieving the strongest overall performance among PLSR, Cubist, from-scratch CNNs, supervised transfer and SSL, without task-specific gradient training.

Its strong OSSL performance further showed that the expanded TabPFN-3 context can extend from small regional calibrations to large spectral libraries without sample subsampling or spectral compression. Together, these findings position TabPFN as a potential new default for soil-spectroscopy modelling: a deep-learning solution that retains the capabilities of modern neural architectures while addressing the sample-size limitation that has constrained conventional architectures in regional soil MIR calibration.

References

Barkov, V., Schmidinger, J., Gebbers, R., Atzmueller, M., 2026. Modern neural networks for small tabular datasets: the new default for field-scale digital soil mapping? European Journal of Soil Science 77, e70299. https://doi.org/10.1111/ejss.70299

Barnes, R.J., Dhanoa, M.S., Lister, S.J., 1989. Standard normal variate transformation and de-trending of near-infrared diffuse reflectance spectra. Applied Spectroscopy 43, 772–777. https://doi.org/10.1366/0003702894202201

Baumann, P., Lee, J., Frossard, E., Schönholzer, L.P., Diby, L., Hgaza, V.K., Kiba, D.I., Sila, A., Sheperd, K., Six, J., 2021. Estimation of soil properties with mid-infrared soil spectroscopy across yam production landscapes in West Africa. SOIL 7, 717–731. https://doi.org/10.5194/soil-7-717-2021

Behrens, T., Viscarra Rossel, R.A., Ramirez-Lopez, L., Baumann, P., 2022. Soil spectroscopy with the Gaussian pyramid scale space. Geoderma 426, 116095. https://doi.org/10.1016/j.geoderma.2022.116095

Dosovitskiy, A., Beyer, L., Kolesnikov, A., Weissenborn, D., Zhai, X., Unterthiner, T., Dehghani, M., Minderer, M., Heigold, G., Gelly, S., Uszkoreit, J., Houlsby, N., 2021. An image is worth 16 x 16 words: transformers for image recognition at scale. International Conference on Learning Representations. https://openreview.net/forum?id=YicbFdNTTy

Grinsztajn, L., Flöge, K., Key, O., Birkel, F., Jund, P., Roof, B., Manium, M., Hoo, S.B., Bühler, M., Garg, A., Safaric, D., Robertson, J., Jäger, B., Alessi, S., Hayler, A., Moroshan, V., Purucker, L., Singer, P., Arazi, A., Siems, J., Metzen, J.H., Grab, G., Erickson, N., Guo, S., Kalfon, E., Bing, S., Salinas, D., Cornu, C., Wehrhahn, L.C., Kriuchkova, D., Kaya, K., Sidhoum, L., Salmon, M., Chen, J., Hulsebos, M., LeCun, Y., Müller, S., Schölkopf, B., Gambhir, S., Hollmann, N., Hutter, F., 2026. TabPFN-3: technical report. arXiv preprint arXiv:2605.13986. https://arxiv.org/abs/2605.13986v2

Hollmann, N., Müller, S., Purucker, L., Krishnakumar, A., Körfer, M., Hoo, S.B., Schirrmeister, R.T., Hutter, F., 2025. Accurate predictions on small data with a tabular foundation model. Nature 637, 319–326. https://doi.org/10.1038/s41586-024-08328-6

Huang, Y.-C., Padarian, J., Ng, W., Minasny, B., McBratney, A.B., 2026. Zero-shot inference with tabular prior-data fitted network (TabPFN) for soil MIR spectral analysis. Geoderma 471, 117880. https://doi.org/10.1016/j.geoderma.2026.117880

Hume, R., Marschner, P., Mason, S., Schilling, R.K., Mosley, L.M., 2024. Using mid-infrared spectroscopy as a tool to monitor responses of acidic soil properties to liming: case study from a dryland agricultural soil trial site in South Australia. Precision Agriculture 25, 1340–1359. https://doi.org/10.1007/s11119-024-10114-3

Khiari, L., 2025. Nouveau système intelligent de diagnostic de l'acidité, de la qualité des amendements et de recommandation d'application calcique (DAQARA) [WWW Document]. MAPAQ Grandes cultures webinar, 21 February 2025. Agri-Réseau. URL https://www.agrireseau.net/grandescultures/documents/115297/ (accessed 19 August 2026).

Kuhn, M., Quinlan, R., 2023. Cubist: rule- and instance-based regression modeling. R package. https://doi.org/10.32614/cran.package.cubist

LeCun, Y., Bengio, Y., Hinton, G., 2015. Deep learning. Nature 521, 436–444. https://doi.org/10.1038/nature14539

Leng, K., Jeffery, S., Panagos, P., Nissen-Meyer, T., 2026. LUCAS-MEGA: a large-scale multimodal dataset for representation learning in soil-environment systems. arXiv preprint arXiv:2605.04323. https://arxiv.org/abs/2605.04323

Liu, L., Ji, M., Buchroithner, M., 2018. Transfer learning for soil spectroscopy based on convolutional neural networks and its application in soil clay content mapping using hyperspectral imagery. Sensors 18, 3169. https://doi.org/10.3390/s18093169

Mishra, P., Passos, D., 2021. Deep calibration transfer: transferring deep learning models between infrared spectroscopy instruments. Infrared Physics & Technology 117, 103863. https://doi.org/10.1016/j.infrared.2021.103863

Mishra, P., Passos, D., Marini, F., Xu, J.-L., Amigo, J.M., Gowen, A.A., Jansen, J.J., Biancolillo, A., Roger, J.-M., Rutledge, D.N., Nordon, A., 2022. Deep learning for near-infrared spectral data modelling: hypes and benefits. TrAC Trends in Analytical Chemistry 157, 116804. https://doi.org/10.1016/j.trac.2022.116804

Mokere, R., Ghassan, M., Barra, I., 2026. Soil spectroscopy improves mid infrared soil property prediction through optimized preprocessing and variable selection. Frontiers in Soil Science 6, 1760011. https://doi.org/10.3389/fsoil.2026.1760011

Ng, W., Minasny, B., Montazerolghaem, M., Padarian, J., Ferguson, R., Bailey, S., McBratney, A.B., 2019. Convolutional neural network for simultaneous prediction of several soil properties using visible/near-infrared, mid-infrared, and their combined spectra. Geoderma 352, 251–267. https://doi.org/10.1016/j.geoderma.2019.06.016

Ng, W., Minasny, B., Mendes, W.d.S., Demattê, J.A.M., 2020. The influence of training sample size on the accuracy of deep learning models for the prediction of soil properties with near-infrared spectroscopy data. SOIL 6, 565–578. https://doi.org/10.5194/soil-6-565-2020

Padarian, J., Minasny, B., McBratney, A.B., 2019. Transfer learning to localise a continental soil vis-NIR calibration model. Geoderma 340, 279–288. https://doi.org/10.1016/j.geoderma.2019.01.009

Prior Labs, 2026. TabPFN: foundation model for tabular data [WWW Document]. GitHub repository. URL https://github.com/PriorLabs/TabPFN (accessed 4 August 2026).

Safanelli, J.L., Hengl, T., Parente, L.L., Minarik, R., Bloom, D.E., Todd-Brown, K., Gholizadeh, A., Mendes, W.d.S., Sanderman, J., 2025. Open Soil Spectral Library (OSSL): building reproducible soil calibration models through open development and community engagement. PLOS ONE 20, e0296545. https://doi.org/10.1371/journal.pone.0296545

Savitzky, A., Golay, M.J.E., 1964. Smoothing and differentiation of data by simplified least squares procedures. Analytical Chemistry 36, 1627–1639. https://doi.org/10.1021/ac60214a047

Shoemaker, H.E., McLean, E.O., Pratt, P.F., 1961. Buffer methods for determining lime requirement of soils with appreciable amounts of extractable aluminum. Soil Science Society of America Proceedings 25, 274–277. https://doi.org/10.2136/sssaj1961.03615995002500040014x

Stenberg, B., Viscarra Rossel, R.A., Mouazen, A.M., Wetterlind, J., 2010. Visible and near infrared spectroscopy in soil science, in: Advances in Agronomy, vol. 107. Elsevier, pp. 163–215. https://doi.org/10.1016/S0065-2113(10)07005-7

Sun, L., Safanelli, J.L., Sanderman, J., Georgiou, K., Brungard, C., Grover, K., Hopkins, B.G., Liu, S., Bremer, P.-T., 2026. Self-supervised and multi-fidelity learning for extended predictive soil spectroscopy. Geoderma 468, 117764. https://doi.org/10.1016/j.geoderma.2026.117764

Vaswani, A., Shazeer, N., Parmar, N., Uszkoreit, J., Jones, L., Gomez, A.N., Kaiser, Ł., Polosukhin, I., 2017. Attention is all you need. Advances in Neural Information Processing Systems 30. https://proceedings.neurips.cc/paper/7181-attention-is-all-you-need

Viscarra Rossel, R.A., Walvoort, D.J.J., McBratney, A.B., Janik, L.J., Skjemstad, J.O., 2006. Visible, near infrared, mid infrared or combined diffuse reflectance spectroscopy for simultaneous assessment of various soil properties. Geoderma 131, 59–75. https://doi.org/10.1016/j.geoderma.2005.03.007

Wan, M., Yan, T., Xu, G., Liu, A., Zhou, Y., Wang, H., Jin, X., 2023. MAE-NIR: a masked autoencoder that enhances near-infrared spectral data to predict soil properties. Computers and Electronics in Agriculture 215, 108427. https://doi.org/10.1016/j.compag.2023.108427

Wold, S., Sjöström, M., Eriksson, L., 2001. PLS-regression: a basic tool of chemometrics. Chemometrics and Intelligent Laboratory Systems 58, 109–130. https://doi.org/10.1016/S0169-7439(01)00155-1

Zhong, L., Guo, X., Xu, Z., Ding, M., 2021. Soil properties: Their prediction and feature extraction from the LUCAS spectral library using deep convolutional neural networks. Geoderma 402, 115366. https://doi.org/10.1016/j.geoderma.2021.115366